Journal of Supramolecular Structure 5:475–495 (1976)

# Comparison of the Structural and Chemical Composition of Giant T-Even Phage Heads

U. Aebi, R. K. L. Bijlenga, B. ten Heggeler, J. Kistler, A. C. Steven, and P. R. Smith

*Abteilung Mikrobiologie, Biozentrum der Universität Basel, Klingelbergstrasse 70, CH-4056, Basel, Switzerland*

A study has been made of the structure of the capsids of T4D giant phage produced from mutants in gene 23 and temperature-sensitive mutants in gene 24, and T4D and T2L giant phage formed by the addition of L-canavanine followed by an L-arginine chase in the growth medium.

All the giant phage capsids have been shown to be built according to the same geometrical architecture. This consists of a near-hexagonal surface net, lattice constant 129.5 Å, folded into a left-handed T = 13 prolate icosahedron elongated along one of its fivefold symmetry axes. Their only apparent difference from wild-type T-even phage capsids is their abnormally elongated tubular part.

A comparison of the capsomere morphologies and protein compositions of the giant phage capsids showed that all T4D giants are identical but differ from T2L: The T4D capsomere has a complex (6 + 6 + 1)-type morphology, whereas the T2L has a simple 6-type. T2L phage, however, lack two capsid proteins, "soc" and "hoc", present in T4D. The difference in capsomere morphology can therefore be related to the difference in the protein compositions of these two phage.

Possible differences between the initiation and means of length regulation of giant phage heads and the aberrant polyheads are discussed.

Key words: **T4 giant phage, morphogenesis, optical/computer image processing, protein composition, phage capsid structure, phage head length determination**

## INTRODUCTION

Giant phage are a polymorphic variant of bacteriophage T-even which is characterised by an abnormal elongation of the wild-type capsid. A variety of means have been used to produce giants (1–4), but in all cases the yield is only a few percent of the total particle yield.[1] Giants are most likely to be produced as a result of a perturbation of the mechanism regulating the length of the normal phage capsid (1, 2, 4–6) but the nature of this perturbation at the molecular level is unknown at present.

[1] This percentage indicates that x% of the P23 molecules associated with the total particle yield in the lysate are assembled in the form of giant phage.

Received September 13, 1976, accepted November 16, 1976

 

The greater length of the giant capsids allows their capsid architecture and fine structure to be studied using image processing of electron micrographs (4, 7, 8). Recently Ishii and Yanagida (8) were able to correlate structural changes in canavanine induced-T4 giant capsids with the presence, or absence, of proteins bound into the capsid stoichiometrically with P23*. This they did by comparing optical filtrations of micrographs of T4 giants induced from wild-type with filtrations of giants induced from phage with mutations in the genes coding for two dispensible capsid proteins that they called soc ($M_r$ = 10,000) and hoc ($M_r$ = 40,000). Soc is most likely to be identical with the $M_r$ = 11,000 protein which Forrest and Cummings (9) found to be present in T4D but absent from T2L capsids.

In this investigation we have undertaken a comparative study of the different types of giant T-even phage to establish the structural relationship between the normal and giant phage heads, and to see whether differences in the gross structure or capsomere morphologies of these giants can be correlated with their respective protein compositions or means of generation. The structural analysis was performed by electron microscopy using different methods of specimen preparation and supplemented with optical and computer image processing. The protein composition was determined by gel electrophoresis of purified tyrosine-iodinated samples followed by autoradiography.

## EXPERIMENTAL PROCEDURES

### a) Bacterial and Phage Strains

Escherichia coli $B^E$ was used for stock preparations, plaque assays and as the host bacterium. Phage mutants T4D·23 (ptg 19–80, ptg 19–2, and ptg 191) and several mutants affecting the three internal proteins of phage T4D were kindly provided by Dr. A. Doermann and Dr. L. W. Black, respectively. Phage strains $T2L^+$, $T4D^+$, and T4D·24 (tsB86) were taken from our laboratory collection.

### b) Culture Techniques

The media used were described previously (10). The different types of giant phage were prepared according to the procedures given by the following authors: For the T4D·23-giants (mutations in gene 23: ptg 19-80, ptg 19-2, ptg 191): Doermann et al. (1). For the T2L·can- and T4D·can-giants: Cummings et al. (3). For the T4D·24-giants: Bijlenga et al. (4). Giant phage were purified on a step gradient made with different percentages of CsCl, $D_2O$ and glycerol (3, 4).

### c) Electron Microscopy

Unless otherwise stated, normal and giant T-even phage used for electron microscopy were kept in Tris·HCl buffer (pH 7.5) in concentrations ranging between $10^9$ and $10^{10}$ particles/ml.

(i) Normal and giant T-even phage used for high-resolution electron microscopy were prepared and observed as described by Bijlenga et al. (4). As negative strains, 1% uranyl acetate (UA), pH 4.5, 2% phosphotungstic acid (PTA), pH 4.5, and 2% sodium phosphotungstate (NaPT), pH 7.2, were used.

(ii) The handedness of the folding of the surface lattice of giant T-even phage was determined by freeze-drying and shadowing them. Giant phage (about $10^{10}$ giants/ml) were

adsorbed on glow-discharged carbon-coated collodion grids and washed several times by floating the grids on drops of distilled water. The grids were then put upside down on a stack of wet filter paper to form a very thin layer of water (20–30 $\mu$ thick). After a few seconds the grids were immersed into liquid nitrogen and put on a precooled specimen holder that was then transferred into a Balzers freeze fracture apparatus (BA511M). Sublimation was carried out at an object stage temperature between −30 and −40°C using the liquid-nitrogen-cooled knife arm as an anticontamination device. The vacuum was kept better than $5 \cdot 10^{-7}$ torr. Shadow casting with tungsten was done with an electron gun source at elevation angles of either 15° or 30°. The amount of tungsten deposited was measured with a quartz film-thickness monitor; the average thickness on the horizontal being standardised to about 6 Å. For stabilization, and to prevent secondary air drying due to atmospheric water vapor, carbon was evaporated from the vertical. The vacuum during this evaporation was about $4 \cdot 10^{-6}$ torr.

#### d) Magnification Calibration

The magnifications of all micrographs were calibrated relative to the spacing of the striations of the extended T4 tail sheath, assumed to be 38 Å (4, 7, 11, 12). T2 and T4, normal and giant phage tails were cross-calibrated using different preparation methods, but no significant differences were found.

#### e) Optical Diffraction and Filtering

Optical processing of electron micrographs of the different types of giant T-even phage, prepared as described in section (c) (i), was performed as outlined by Steven et al. (11, 12) and Bijlenga et al. (4). Except for freeze-dried and shadowed preparations, all optical filtrations were twofold rotationally symmetrised (4, 11).

#### f) Computer Filtrations

The giant particles that gave the best optical filtrations were enlarged onto Typon Rototyp FRK film so that the near-equatorial lattice constant of the surface lattice to be filtered was 1.6 mm. The film was mounted on the drum of an Optronics Photoscan (P-1000) so that it could be scanned parallel to the near-equatorial lattice vector. An area of the enlarged particle, which contained the part used for optical filtration, was digitized on a 50 $\mu$ scanning raster (corresponding to an image sampling distance of about 4 Å) and then transferred via magnetic tape to the IBM 370-158 computer at F. Hoffmann-La Roche, Basel. Filtration and sixfold rotational symmetrisation were performed as described in the Appendix to give an (unrescaled) array 56 × 32 points containing two unit cells of the hexagonal lattice. A photographic-quality negative was then produced on an Optronics Photomation (P-1700) using the 50 $\mu$ raster, by periodically continuing this basic array and bilinearly interpolating it both to correct the scaling in the two directions and to give a sampling rate ten times greater than that of the basic filtered array. Power loss at each stage of the filtration process was calculated after excluding the zero order since this only contributes a constant background.

#### g) Protein Composition

For reasons discussed elsewhere (4) the protein composition of normal and giant T2 and T4 phage was determined by applying purified samples iodinated with $^{131}I$ to SDS

polyacrylamide gel electrophoresis (13), followed by autoradiography (4). Since we were primarily interested in those proteins that it was anticipated would be present in stoichiometric amounts to the major head protein P23*, we had only to compare the amounts of the various proteins relative to the amount of P23* for normal and giant phage. However, it was not necessary to know the absolute amounts of these proteins. Note that quantitation by the iodination procedure is only valid if the tyrosine residues of the different constituent proteins are labeled to the same extent in wild-type and giant phage.

## RESULTS

### a) Gross Morphology of the Giants

Typical examples of T4D·23 (ptg 19-80) and T2L·can-giants together with their wild-types are shown in Fig. 1.

Of all the different types investigated, only the T4D·24-giants have a narrow length distribution, peaking sharply at (10.9 ± 2.2) wild-type head lengths (4). It was found (3, 4) that T2L·can-, T4D·can- and T4D·24-giants tend to have two tails when they are longer than about seven normal head lengths. We have also found this to be true for the T4D·23-giants. About 10% of the two-tailed T2L·can-giants appeared to be of the apical-nonapical type (see Fig. 2b), but for all other types more than 97% of the two-tailed giants we analysed were of the apical-apical type (see Fig. 1b).

Giants negatively stained with 1% UA appeared roughly 1.5 times wider than normal phage, which were mixed with the giant phage (Fig. 1a, b). In order to test whether these giants were completely flattened, negatively stained samples were shadowed with tungsten at low angle (~ 8°). Figure 2c shows the same stretch of a giant phage capsid before and after shadowing. The upper surfaces of these shadowed giants were seen to be essentially flat but with small undulations. Their (flattened) thicknesses, calculated from the length of the shadows they cast, lay between 50 and 80 Å. Giant phage soaked in saturated UA for 20 min prior to negative staining (1) appeared to have the same width as normal phage present in the sample (Fig. 2a), probably due to the UA having cross-linked their DNA (14). Low-angle shadowing (~8°) of these samples showed both the giant and normal phage to be nearly as thick as they were wide (Fig. 2b).

We therefore concluded that giant and normal T-even phage have the same unflattened capsid diameter of about 745 Å. The apparently increased width of a negatively stained giant prepared without presoaking it in saturated UA appears to be due to the flattening of the cylindrical part of the head onto the grid while maintaining its circumference.

### b) The Giant Capsid Geometry

(i) The parameters characterising the surface lattice of the tubular part of the giant capsid are common to all giant T-even phage.

The tubular parts of more than 50 giants of each type, which were evenly stained and flattened over their whole length (see Fig. 1a and 1b) were optically diffracted. Examples representative for T4 and T2 giant phage are shown in Fig. 1c and 1d, respectively. In both cases, the diffraction spots could be associated with one or the other of two near-hexagonal reciprocal lattices, which were almost exactly mirror-symmetric with respect to the meridian. For both T2 and T4 giants, diffraction patterns were often obtained where the set of spots arising from one of the two sides of the flattened

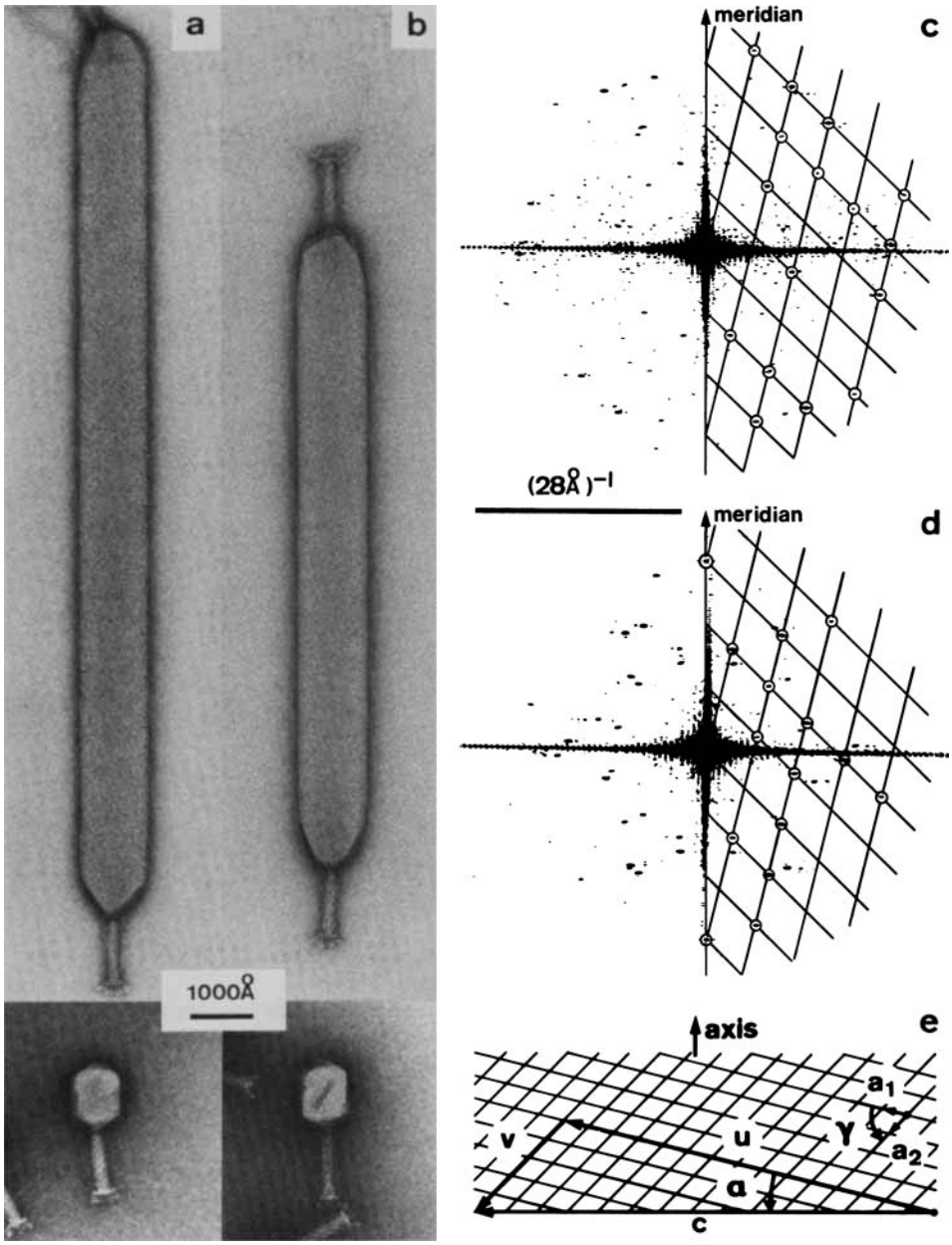


Fig. 1. Electron micrographs of negatively stained (1% UA, pH 4.5) wild-type and giant T-even phage: a) T4D·23 (ptg 19-80)-giant together with T4D wild-type; b) T2L·can-giant together with T2L wild-type. Optical diffraction patterns coming from rectangular stretches of the tubular parts of giant T-even phage containing about 150 unit cells. The set of diffraction spots that can be assigned to the near side of the particle (see text) is indexed according to a near-hexagonal reciprocal lattice: c) T4D·23 (ptg 19-80)-giant; d) T2L·can-giant; e) Schematic representation of a stretch of unwrapped near-hexagonal surface net of the tubular part of giant T-even phage with a left-handed folding corresponding to a circumference vector c with (u,v) coordinates (15, 5). $a_1$ and $a_2$ are the near-equatorial and near-axial lattice vectors, respectively, $\gamma$ the angle between $a_1$ and $a_2$ and $\alpha$ the pitch angle.

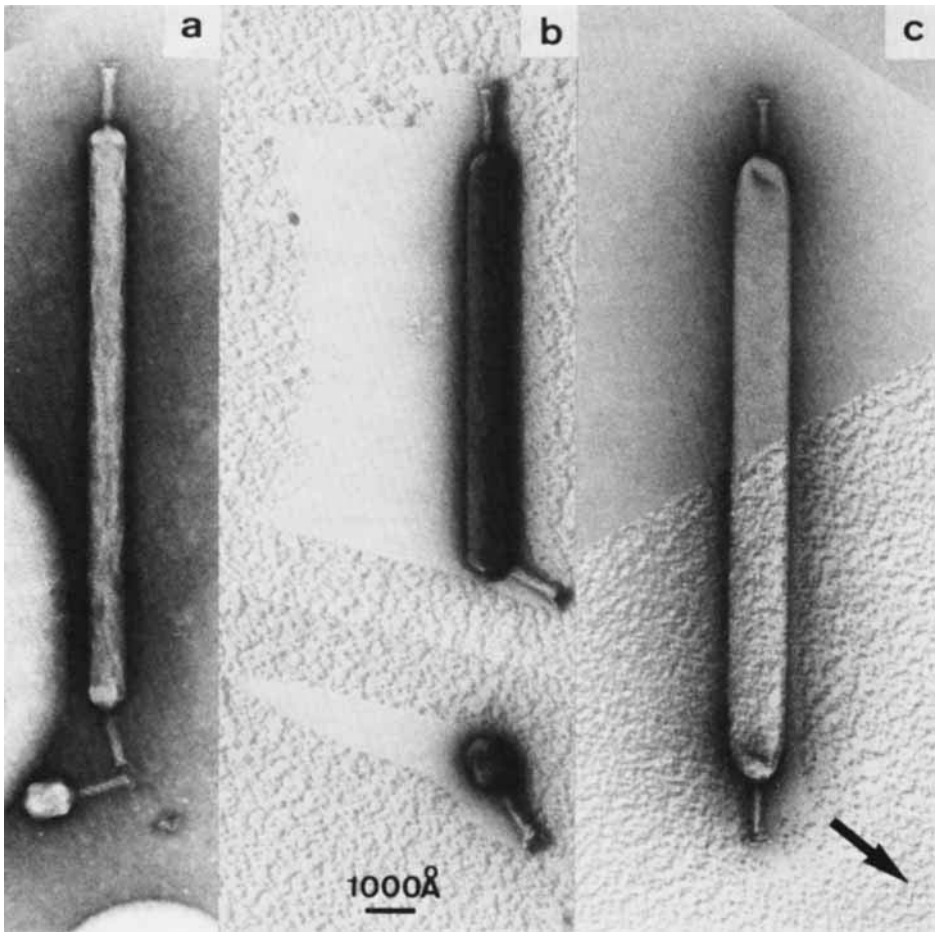


Fig. 2. a) Electron micrograph of normal and giant T4D phage that have been soaked in saturated uranyl acetate for 20 min prior to being washed and negatively stained with 1% UA, pH 4.5. b) Sample containing normal and wild-type T4D phage stained as described in a) and tungsten-shadowed at low angle (~ 8°). c) The same stretch of a giant T4 phage negatively stained with 1% UA, pH 4.5, before (top) and after (bottom) tungsten shadowing at low angle (~ 8°).

cylindrical lattice was more complete and significantly stronger than the set coming from the other side. In all such cases the known left-handed pitch of the lattice (see section b, iii) allowed the "strong" side to be identified, without exception, as the side in contact with the supporting film (called the "near" side). Particles that gave rise to such asymmetric diffraction patterns appeared not to have been significantly penetrated by negative stain.

Twenty or more particles of each type giving diffraction patterns that indicated good preservation of the near side of the tubular part of the head were used for a statistical analysis of the parameters characterising the giant phage surface lattice.

The two lattice constants $a_1$ and $a_2$, the angle between them $\gamma$, and the pitch angle $\alpha$ (see Fig. 1e) were measured from the optical diffraction patterns following the procedure and conventions described by Bijlenga et al. (4). The average width $d_g$ of the tubular part

was directly measured on the micrographs. The mean values of $a_1$, $a_2$, $\gamma$, $\alpha$, and $d_g$ together with their standard deviations are listed in Table I for all types of giant phage analysed and for different ways of preparing them for the electron microscope. In addition, we have calculated and tabulated an average lattice constant $\bar{a}$, the u/v ratio, and an "ideal" flattened width $d_{flat}$. The formulae used for these calculations are given in the caption of Table I.

(ii) The surface lattices of all giant phage have left-handed foldings.

Since negatively stained preparations of the giant phage surface lattice did not allow us to determine its handedness, we freeze-dried and shadowed giant phage as described in section (c) of Experimental Procedures.

When T2L·can-giants are freeze-dried and shadowed at an elevation angle of about 30°, capsomeres are clearly seen on their surface. These capsomeres are arranged in a quasi-p6 lattice with a left-handed 14° pitch (Fig. 3a), confirmed by indexing their optical diffraction patterns (Fig. 3c).

T4 giants freeze-dried and shadowed at an elevation angle of 30° never showed visible capsomeres or striations. When the elevation angle was reduced to 15°, however, some giants were found whose tubular parts (Fig. 3b) gave indexable optical diffraction patterns (Fig. 3d). Again, without exception, all T4 giant surface lattices analysed in this way were left-handed.

From the results accumulated in this section, we conclude that the tubular part of all giant T-even phage is built of a closed near-hexagonal lattice having an average lattice constant of (129.6 ± 0.5) Å and a left-handed folding with (u,v) coordinates of (15, 5) (Fig. 1e).

(iii) All giant phage heads have fivefold axial rotational symmetry.

It has been shown previously for T4D·24-giants (4) that the measured widths and calculated u/v ratios could best be fitted by a circumference vector of the tubular part having (u,v) coordinates of (15, 5), implying fivefold axial rotational symmetry. The tabulated widths and u/v ratios given in Table I clearly show that all the different types of giant phage have very similar properties in this respect, and therefore we conclude that all giant T-even phage are abnormally elongated along a fivefold rotational symmetry axis.[2]

### c) The Unit Cell Morphology of the Giant Surface Lattice

Areas of micrographs containing 100–200 unit cells of the surface lattice of the tubular part of up to 10 giants of each type that had given good optical filtrations were then computer-filtered. In all cases good agreement between the optical and computer filtrations was obtained.

(i) All T4 giants have a (6 + 6 + 1)-type unit cell morphology.

Computer filtered areas (containing 7.5 unit cells each) representative of the different types of T4 giants analysed (24, 23(ptg 19-20), 23(ptg 19-2), 23(ptg 191), T4D·can) are shown in Fig. 4a–e. They all possess a characteristic (6 + 6 + 1)-type unit cell morphology (4, 8) consisting of a strong central stain-excluding region surrounded by six fainter ones at a mean radius of about 37 Å and with a mean orientation angle of about

[2] Using a method similar to that proposed by Lake and Leonard (33), we determined computationally that both the T2 and T4 giant capsids had odd rotational symmetry about their long axes. It is important to realize, however, that the computational determination of the axial rotational symmetry as being either odd or even is not necessarily a particularly powerful method for discriminating between different possible choices for u and v. In our case, the values u = 16, v = 4 could be said to be within the extreme range of the variation allowed by the data presented in Table II.

TABLE I. Surface Lattice Parameters of the Cylindrical Part of the Different Types of Giant T-even Phage

| Type | Preparation | N | $a_1$ (Å) | $a_2$ (Å) | $\gamma$ (°) | $\bar{a}$ (Å) | $\alpha$ (°) | u/v | $d_g$ (Å) | $d_{flat}$ (Å) |
|---|---|---|---|---|---|---|---|---|---|---|
| T4D·24 | 1% UA, pH 4.5 | 50 | 127.5 ± 2.8 | 129.4 ± 1.5 | 60.8 ± 1.5 | 129.0 ± 2.0 | 14.0 ± 0.5 | 3.06 | 1108 ± 24 | 1149 |
| T4D·24 ghosts | 1% UA, pH 4.5 | 25 | 128.3 ± 1.1 | 129.9 ± 1.0 | 60.8 ± 0.6 | 129.6 ± 0.7 | 14.2 ± 0.3 | 3.01 | 1123 ± 20 | 1156 |
| T4D·24 | freeze-dried + shadowed (≮ 15°) | 15 | 126.8 ± 1.8 | 128.1 ± 1.8 | 61.0 ± 1.6 | 128.1 ± 1.2 | 14.4 ± 0.5 | 2.96 | 1125 ± 32 | 1141 |
| T4D·23 (ptg 19-2) | 1% UA, pH 4.5 | 25 | 130.3 ± 1.1 | 130.0 ± 0.8 | 59.7 ± 0.6 | 129.9 ± 0.6 | 13.7 ± 0.3 | 3.03 | 1100 ± 24 | 1175 |
| T4D·23 (ptg 19-80) | 1% UA, pH 4.5 | 25 | 126.8 ± 2.0 | 129.9 ± 1.7 | 61.9 ± 1.1 | 129.7 ± 1.2 | 14.3 ± 0.3 | 3.06 | 1075 ± 35 | 1140 |
| T4D·23 (ptg 191) | 1% UA, pH 4.5 | 25 | 131.2 ± 1.6 | 130.4 ± 1.2 | 59.3 ± 0.8 | 130.3 ± 0.8 | 13.8 ± 0.3 | 2.98 | 1090 ± 27 | 1184 |
| T4D·can | 1% UA, pH 4.5 | 25 | 126.8 ± 4.8 | 130.6 ± 3.8 | 62.8 ± 2.9 | 129.9 ± 2.8 | 14.8 ± 0.8 | 3.00 | 1104 ± 37 | 1138 |
| T2L·can | 1% UA, pH 4.5 | 50 | 128.3 ± 1.5 | 129.0 ± 1.1 | 60.5 ± 0.6 | 129.0 ± 1.0 | 14.1 ± 0.3 | 2.99 | 1108 ± 22 | 1156 |
| T2L·can ghosts | 1% UA, pH 4.5 | 25 | 128.7 ± 1.0 | 129.5 ± 0.7 | 60.7 ± 0.6 | 129.6 ± 0.6 | 14.0 ± 0.3 | 3.02 | 1120 ± 25 | 1159 |
| T2L·can | freeze-dried + shadowed (≮ 30°) | 15 | 125.3 ± 1.3 | 128.1 ± 1.3 | 61.7 ± 0.5 | 127.8 ± 1.0 | 14.3 ± 0.4 | 3.05 | 1095 ± 41 | 1128 |

N = number of particles measured per sample $a_1$, $a_2$, $\gamma$, $\alpha$, $d_g$: see text and Fig. 1(e).

$$\bar{a} = \left(\frac{a_1 \cdot a_2 \cdot \sin\gamma}{\sin 60°}\right)^{1/2}$$

$$u/v = \left(\frac{\sin\gamma}{\sin\alpha} - \cos\gamma\right) \cdot \frac{a_2}{a_1}$$

$d_{flat} = \frac{c}{2}$, where $c = [(u \cdot a_1 + v \cdot a_2 \cdot \cos\gamma)^2 + (v \cdot a_2 \cdot \sin\gamma)^2]^{1/2}$ is the circumference of the tubular part (see Fig. 1e).

All lattice parameters are expressed as mean values together with their standard deviations.

When 2% PTA, pH 4.5, or 2% NaPT, pH 7.2, was used as a negative stain, no significant changes in the lattice parameters were observed.

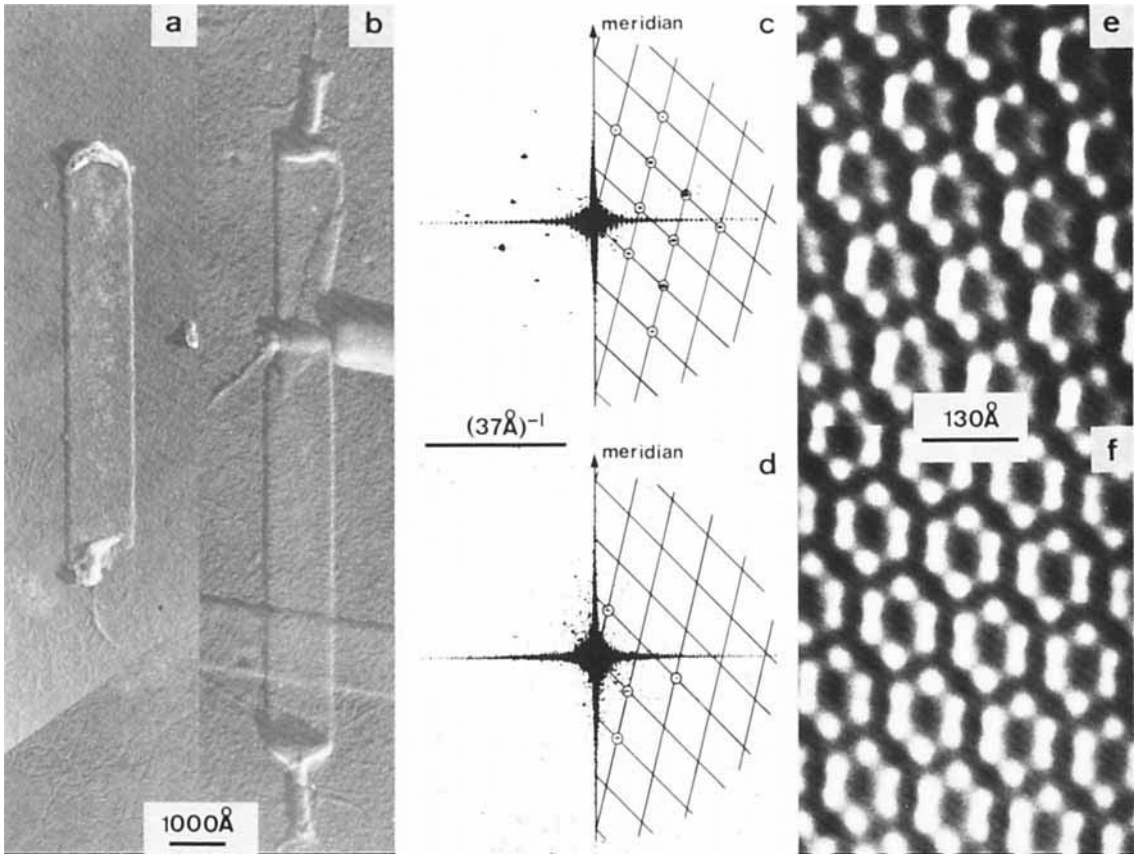


Fig. 3. Electron micrographs of freeze-dried and shadowed giant T-even phage: a) T2L·can-giant; elevation angle: 30°; b) T4D·24-giant; elevation angle: 15°. Optical diffraction patterns coming from a rectangular stretch of the tubular part of giant T-even phage containing about 150 unit cells. The diffraction spots have been indexed according to a left-handed near-hexagonal reciprocal lattice: c) T2L·can-giant shown in a); d) T4D·24-giant shown in b); e) filtered area of a rectangular stretch containing about 150 unit cells of the tubular part of T2L·can-giant shown in a), f) twofold rotationally averaged area of filtration shown in e). The twofold rotational averaging was done as described in Bijlenga et al. (4).

22° (see Table II). The quasi-threefold rotational symmetry axes of the lattice are occupied by stain-excluding trimers that bridge three adjacent capsomeres.

It is important to note that the range of variation in unit cell morphology among the filtrations of the different types of T4 giants is no greater than that among different filtrations of giants of a given type. We therefore conclude that at our working resolution of about 30 Å no significant differences can be observed between the unit cell morphologies of the surface lattices of the different types of T4 giants. Since little periodically repeating information was preserved when T4 giants were freeze-dried and shadowed (Fig. 3b), no filtrations were made from these micrographs.

(ii) T2L giants have a 6-type unit cell morphology.

Figure 4f shows a computer-filtered area representative of T2L·can-giants. These have a simple 6-type unit cell morphology consisting of six strong stain-excluding regions at a mean radius of about 42 Å (Table II), around the local quasi-sixfold rotational symmetry axes of the lattice. The capsomere orientation angle is indistinguishable from that of T4 giants (~ 22.5°). A similar capsomere morphology is found when optically filtering freeze-dried and shadowed samples (Fig. 3a), as shown in Fig. 3e. Figure 3f is a twofold rotationally symmetrised image generated from Fig. 3e. The pronounced capsomere ellipticity found for all filtered particles (Table II) correlated well with the shadowing direction (Fig. 3a): The capsomeres appeared compressed in the shadowing direction and stretched perpendicular to it leaving the mean capsomere diameter (Table II) almost invariant.

Since Ishii and Yanagida (8) found a correlation between the unit cell morphologies seen in filtered images of negatively stained samples and the protein composition of the different types of giant T-even phage, it was important to have a quantitative characterisation of their different capsomere morphologies. A statistical analysis of the capsomere parameters (11, 12) was therefore done for the different types of giant phage. The parameters measured were the capsomere orientation angle $\phi$; the average capsomere diameter $d_c$; the capsomere ellipticity $e_c$; the lattice ellipticity $e_l$; $\delta$, the angle between the major axis of the capsomere ellipse and the particle axis; and $\epsilon$, the angle between the major axes of the capsomere and lattice ellipses. Their mean values and standard deviations are listed in Table II. The capsomere orientation angle appears to be very much the same for all giants (22.2 ± 0.9)°. The mean capsomere diameter is (74.5 ± 0.6) Å when averaging over all giant T4 samples analysed (Table II). This is roughly 9 Å smaller than the mean value measured for T2L·can-giants (83.5 ± 0.5) Å. The average capsomere and lattice ellipticities of all types of giants are only slightly greater than 1, ranging between 1.03 and 1.15 (except for freeze-dried and shadowed T2L·can-giants: 1.31 ± 0.12), the lattice ellipticity being consistently smaller than the capsomere ellipticity. Neither the capsomere nor the lattice ellipse show a preferential orientation relative to the particle axis, although in all cases the major axis of the capsomere ellipse is closer to the particle axis than to the equator ($|\delta| < 45°$: see Table II). No correlation was found between the orientations of the capsomere and lattice ellipses.

### d) Protein Composition

The molecular organisation of the head can only be established when the proteins present in the head shell stoichiometric to P23* have been identified. Our method was to compare the gel patterns of wild-type and giant phage: Those proteins that increased in proportion to P23* in the giants relative to wild-type could be identified as being incorporated with P23* in the elongated tubular part of the giant heads.

TABLE II. Parameters Characterising the Surface Lattice Unit Cell Morphology of the Different Types of Giant T-even Phage

| Type | Preparation | N | $d_c$(Å) | $\phi$(°) | $e_c$ | $e_l$ | $\delta$ (°) | $\epsilon$(°) |
|---|---|---|---|---|---|---|---|---|
| T4D·24 | 1% UA, pH 4.5 | 8 | 75.0 ± 1.8 | 22.4 ± 2.0 | 1.091 ± 0.057 | 1.033 ± 0.023 | 35.5 ± 39.6 | − 17.6 ± 48.2 |
| T4D·24 ghosts | 1% UA, pH 4.5 | 7 | 74.1 ± 2.8 | 21.1 ± 2.0 | 1.132 ± 0.063 | 1.051 ± 0.038 | 20.8 ± 34.2 | − 42.8 ± 34.8 |
| T4D·23 (ptg 19-2) | 1% UA, pH 4.5 | 6 | 74.6 ± 1.5 | 23.5 ± 1.2 | 1.133 ± 0.055 | 1.078 ± 0.027 | − 17.4 ± 30.0 | − 22.5 ± 10.5 |
| T4D·23 (ptg 19-80) | 1% UA, pH 4.5 | 5 | 73.9 ± 1.9 | 21.4 ± 1.3 | 1.153 ± 0.070 | 1.064 ± 0.024 | − 32.7 ± 51.3 | − 64.7 ± 15.6 |
| T4D·23 (ptg 191) | 1% UA, pH 4.5 | 5 | 73.8 ± 2.2 | 22.1 ± 1.7 | 1.087 ± 0.064 | 1.035 ± 0.028 | 11.0 ± 26.8 | − 35.7 ± 11.9 |
| T4D·can | 1% UA, pH 4.5 | 6 | 75.4 ± 0.8 | 21.5 ± 1.5 | 1.090 ± 0.038 | 1.086 ± 0.028 | − 38.1 ± 14.9 | − 33.3 ± 34.2 |
| T2L·can | 1% UA, pH 4.5 | 10 | 83.4 ± 2.6 | 22.8 ± 3.3 | 1.119 ± 0.064 | 1.060 ± 0.051 | − 7.3 ± 46.7 | − 23.8 ± 56.0 |
| T2L·can ghosts | 1% UA, pH 4.5 | | 82.9 ± 2.3 | 22.2 ± 2.8 | 1.121 ± 0.071 | 1.045 ± 0.063 | 19.3 ± 41.3 | − 8.5 ± 48.1 |
| T2L·can | freeze-dried + shadowed (< 30°) | 6 | 84.1 ± 2.4 | 24.1 ± 1.5 | 1.312 ± 0.123 | 1.065 ± 0.047 | − 6.1 ± 27.5 | − 28.3 ± 30.8 |

N = number of particles measured per sample.

$d_c$: average capsomere diameter; $d_c = (d_{c,1} \cdot d_{c,2})^{1/2}$ with $d_{c,1}$ and $d_{c,2}$ being the major and minor axes, respectively, of the ellipse fitted through the capsomere (11). In order to facilitate comparison between the different samples, the average capsomere diameter was scaled relative to an average lattice constant $\bar{a}$ (see Table I) of 129.5 Å for all samples.

$\phi$ = capsomere orientation angle (4, 11)

$e_c$ = capsomere ellipticity; $e_c = d_{c,1}/d_{c,2}$

$e_l$ = lattice ellipticity $e_l = d_{e,1}/d_{e,2}$ with $d_{e,1}$ and $d_{e,2}$ being the major and minor axes of an ellipse fitted to the surface lattice rectors (11).

$\delta$ = angle between particle axis and major axis of capsomere ellipse.

$\epsilon$ = angle between major axes of capsomere and lattice ellipses.

When 2% PTA, pH 4.5, or 2% NaPT, pH 7.2, was used as a negative stain no significant changes in the capsomere parameters were observed.

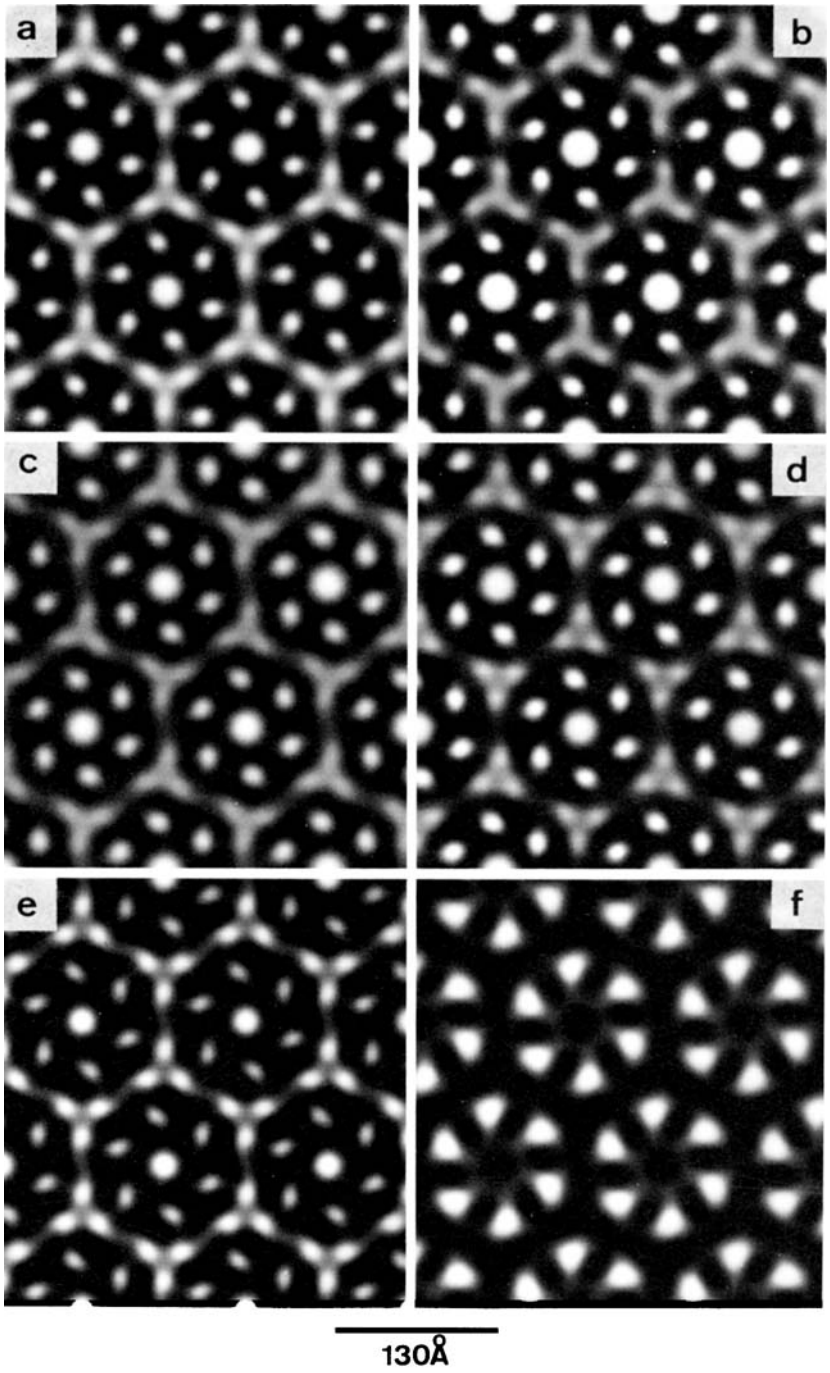


Fig. 4. Areas containing 7.5 unit cells of computer-filtered areas containing 50 unit cells of the near side of the tubular part of giant T-even phage negatively stained with 1% UA, pH 4.5. In all cases the filtered unit cells were sixfold rotationally symmetrised: a) T4D·24-giant; b) T4D·23 (ptg 19-2)-giant; c) T4D·23 (ptg 19-80)-giant; d) T4D·23 (ptg 191)-giant; e) T4D·can-giant; f) T2L·can-giant.

Purified samples of normal and giant phage were iodinated with $^{131}I$ and analysed by SDS polyacrylamide gel electrophoresis followed by autoradiography. We found that for all T4 giants analysed (see Fig. 5c–f) only the proteins PB1, Px, IPIII*, and the proteins migrating with the tracking dye on 10% gels increased in proportion to P23* For T2L giants (see Fig. 5a and 5b), however, only the proteins migrating with the tracking dye increased in proportion to P23*.

In order to separate the different proteins migrating with the tracking dye on 10% gels, we analysed samples on 10–22% gradient gels. In the case of wild-type and giant T4 phage three bands were resolved, all of which increased in proportion to P23* in giants (Fig. 5i and 5j). We identified them with the aid of IPI$^-$, IPII$^-$, IPIII$^-$, and IP0 mutants (Fig. 6a–f), kindly provided by Dr. L. Black, and by using some purified soc protein (Fig. 6j) given to us by Dr. M. Yanagida. The slowest of the three bands represents IPII* (Fig. 6c), the fastest one IPI* (Fig. 6b), and the intermediate one, which we previously called Py (4), is identical with soc (Fig. 6j). Similarly, the proteins migrating with the tracking dye of wild-type and giant T2L phage could be separated into three bands on 10–22% gradient gels (Fig. 5g and 5h; see also Fig. 6g): IPIII* and possibly IPII* and IPI* (the last two not identified). The band seen at the position of soc in the T4D gel (Fig. 6i) was absent in T2L (Fig. 6g). Note also that the IPIII*'s from T2L (Fig. 5g) and T4D (Fig. 5i) do not migrate with the same speed (15) in this gel system.

Some partially purified hoc protein (a gift of Dr. M. Yanagida) was run with T2 and T4 phage on 10–22% gradient gels (Fig. 6h) and was found to comigrate with the T4D phage band that we had previously called Px (4) (Fig. 6i). T2L phage showed a fainter band at this migration distance (Fig. 6g) that was often split into two almost overlapping bands: However, they did not increase in proportion to P23* in T2L giants (Fig. 5g, h). In order to decide whether these bands were related to T4 hoc protein, samples of wild-type T2L and T4D phage together with hoc protein purified as described by Ishii and Yanagida (8) were run on a 12.5% SDS polyacrylamide gel. An immune replica (16) of this gel was made with an anti-T4D·23(ts) serum containing a strong anti-hoc activity kindly provided by Dr. L. Onorato. The serum was precipitated by both the purified hoc protein and the T4D protein comigrating with hoc. No T2L band was able to precipitate the serum.

As in the case of the T4D·24-giants (4), the bands corresponding to the proteins P20 and P24* did not increase in proportion to P23* in the T2 and T4 giants analysed (Fig. 5), showing that they are not incorporated stoichiometrically to P23* into the tubular part of the phage head.

The above results suggest that for wild-type and giant T4 phage only the proteins hoc and soc are likely to be present in amounts stoichiometric to P23* on the head shell. The internal proteins also increase proportionally to P23* in giants; however, it has been shown (17, 18), that they are located within the head. This is also true for PB1 (19), which has been shown to be an internal protein and is injected with the DNA (19–21). Normal and giant T2L phage, on the other hand, lack both soc (8) and hoc. P23* is therefore the only major constituent protein of the tubular part of the T2L head shell.

## DISCUSSION

An important result emerging from this investigation is that the head shells of all giant T2 and T4 phage studied are built according to a common geometrical architecture. Their tubular part can be described as a cylindrically folded near-hexagonal protein lattice

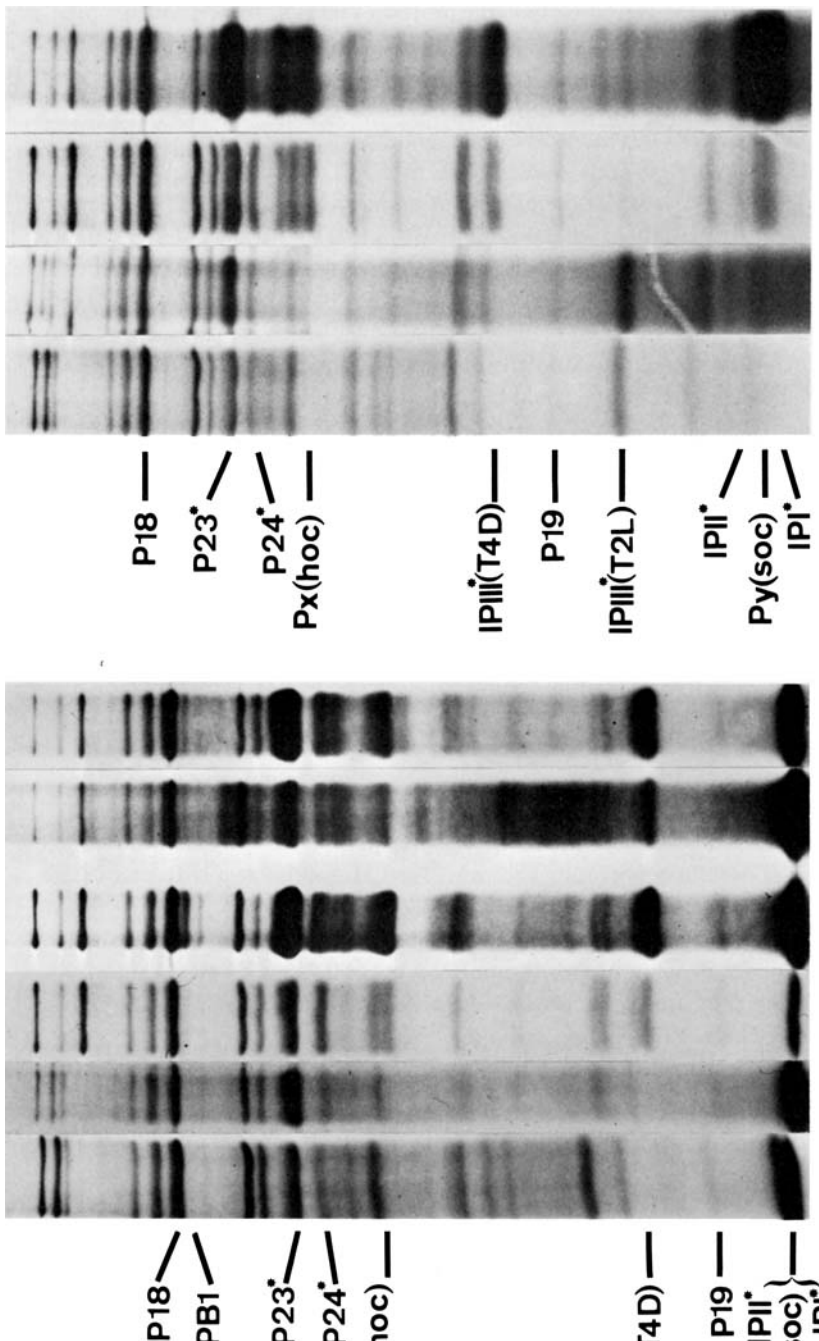


Fig. 5. Autoradiographs of purified wild-type and giant T-even phage iodinated with $^{131}$I prior to application to SDS-containing polyacrylamide gels. The autoradiographs shown in 7a–f were taken from 10% polyacrylamide gels; the ones shown in 7g–j were taken from 10–22% polyacrylamide gradient gels: a) wild-type T2L phage, b) T2L·can-giants, c) wild-type T4D phage, d) T4D·23 (ptg 19-2)-giants, f) T4D·24-giants, g) wild-type T2L phage, h) T2L·can-giants, i) wild-type T4D phage, j) T4D·can-giants.

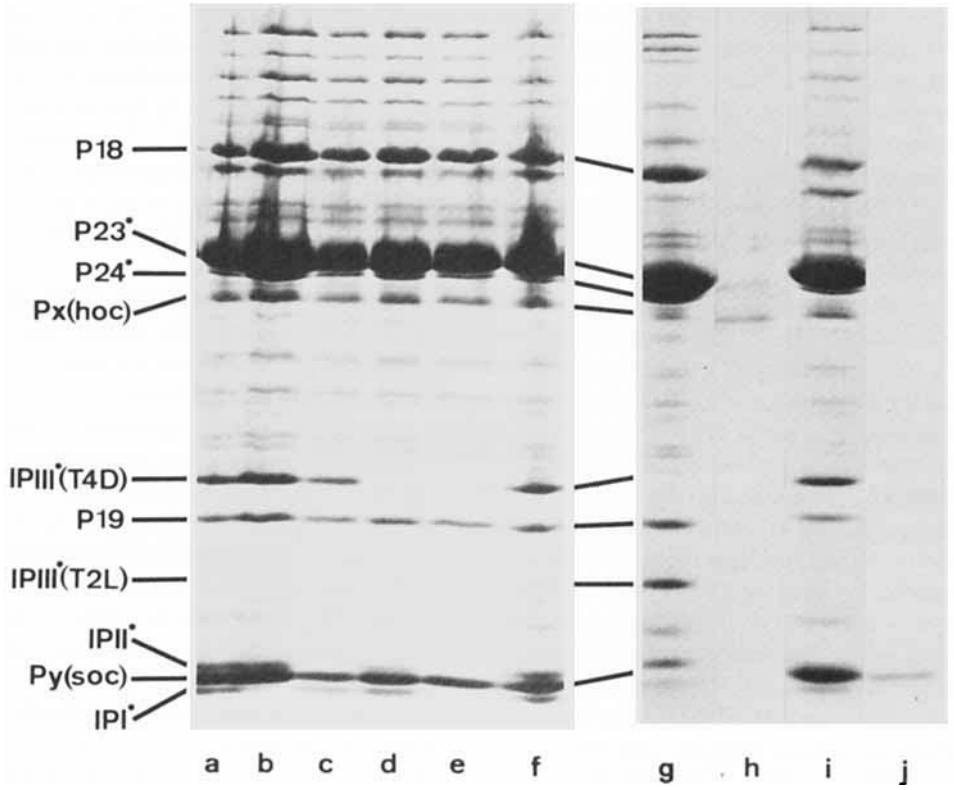


Fig. 6. Identification of the T4D internal proteins IPI*, IPII*, and IPIII* on 10–22% polyacrylamide gradient gels containing SDS using IPI$^-$, IPII$^-$, IPIII$^-$, and IP$^\circ$ mutants: a) T4D wild-type marker, b) IPI$^-$, c) IPII$^-$, d) IPIII$^-$, e) IP$^\circ$, f) T4D wild-type marker. Identification of the proteins Px (hoc) and Py (soc) on 10–22% polyacrylamide gradient gels containing SDS using partially purified hoc and purified soc markers: g) T2L wild-type, h) hoc marker, i) T4D wild-type, j) soc marker.

with an average lattice constant of 129.5 Å. In all cases this lattice has left-handed folding with (u,v) coordinates of (15, 5) (see Fig. 1e), meaning that the tubular part of all giant phage heads has fivefold axial rotational symmetry. This symmetry should also be shared by the two caps closing its ends.

Experimental evidence has been given (7, 22, 23) that the T-even phage capsid can be described geometrically as a prolate icosahedron with T = 13 (7, 23), elongated along one of its fivefold rotational symmetry axes, whose tubular part therefore has (u,v) coordinates of (15, 5). We consequently suggest that the giant phage studied here as well as the isometric (1, 24–26) and intermediate length (1) T-even phage capsids differ from the wild-type capsid geometry only through an abnormal elongation or foreshortening of their tubular part.

Since all giant T4 capsids show the same (6 + 6 + 1)-type capsomere morphology at the resolution (~ 30 Å) of our filtered images, we conclude that the capsomere morphology is not affected by the different means used to induce a malfunction in the mechanism determining phage head length. The difference between the (6 + 6 + 1)-type capsomere

morphology of the T4 giants and the 6-type of the T2L giants can, however, be correlated with differences in the protein composition of their capsids since both wild-type and giant T2L phage lack two proteins, soc and hoc, that are present in amounts stoichiometric to the major capsid protein P23* (8) in both wild-type and giant T4 phage. In fact we have shown elsewhere (27) that the central stain-excluding region of the (6 + 6 + 1)-type capsomere can be associated with one molecule of hoc, and the stain-excluding trimers that bridge the three adjacent capsomeres are associated with three molecules of soc. The latter result is a substantiation of a tentative conclusion drawn previously by Ishii and Yanagida (8).

The observation that the capsomere morphologies of T2L and T4D giant phage are unaltered whether or not the giant capsids are penetrated by negative stain suggests that the structural features giving rise to the observed pattern of stain exclusion are mainly located on the outside of the head shell. Inspection of optically filtered freeze-dried and shadowed T2L giants shows them to have a coarse outer surface with a capsomere morphology correlating well with that visualised in filtrations of negatively stained preparations. Giant T4 capsids, on the other hand, show a very smooth surface when freeze-dried and shadowed. This suggests that both soc and hoc bind to the coarse outer side of the P23* matrix. In fact, we have recently confirmed this by in vitro complementing T2L·can-giants (which are closed structures) with purified proteins hoc and soc (27). Furthermore, we have found that Fab fragments prepared from antibodies directed against hoc bind to the outer side of the stain excluding centers of the (6 + 6 + 1)-type capsomeres of intact T4D giant phage capsids (U. Aebi et al., paper in preparation).

The structure of the giant phage capsids can be contrasted with that of polyheads, which are tubular particles assembled from P23 readily identifiable in lysates of $20^-$, $22^-$, $24^-$, $40^-$ and $IPIII^-$ infected cells (11, 28–31). Steven et al. (11) have shown that while giants have exclusively left-handed (15, 5) lattice foldings, uncapped polyheads have a whole range of right-handed foldings (J. Kistler, reported in Ref. 11) and never have the (15, 5) (u,v) coordinates. Since, as discussed below, we believe the (15, 5) folding to be necessary for the assembly of a normal phage capsid precursor ($\tau$ particle), we define a polyhead to be any tubular P23 or P23* structure whose (u,v) coordinates are not (15, 5). Tubular particles assembled from P23 having the correct (15, 5) folding we have called giant $\tau$ particles (4, 11): These are nearly always capped on at least one end (4; also A.C. Steven, unpublished results).

The finding (11) that certain mutations in genes 20, 22, and 40 produce polyheads exclusively [and therefore, by the above definition, never produce correctly folded (15, 5) tubular structures] shows that the products of these three genes, together with P23, are needed to initiate the correct (15, 5) folding of the P23 lattice. After correct initiation, which is probably associated with the formation of a fivefold T = 13 icosahedral cap, assembly of the tubular part of the capsid would proceed until the correct length is attained and the distal end-cap formed. According to this model, giant phage capsid formation would be the result of a perturbation of the mechanism determining the length of the tubular part of the capsid, rather than a perturbation at the earlier initiation step.

The fact that in $20^-$, $22^-$ and $40^-$ lysates polyheads are formed about 20 min later than the onset of normal phage production in a wild-type infection (10, 29) suggests that their initiation may be quite different from that of normal phage capsids. Furthermore, their aberrant folding precludes them from being normally capped (11). In view of this we doubt that polyheads are subject to the same length determination mechanism as phage;

rather we expect that physical constraints such as the cell dimensions would restrict polyhead length.

How, then, is the normal phage head length determined? Recently Paulson et al. (26) have found two different temperature-sensitive mutations in gene 22 that both produce high frequencies (up to 85%) of isometric phage heads when grown at permissive or intermediate temperature. These results, together with the different means of giant phage production, suggest that the mechanism for determining phage head length is mediated by some interaction between the core proteins and the head shell during polymerisation of the tubular part. At present, however there is no clear evidence as to the nature of this interaction.

Three mechanisms for length determination in general have been proposed but none of them have so far been proven to explain length regulation in a biological system. These mechanisms are called "the template," "cumulated strain," and "Vernier" models (for a recent review see Kellenberger, Ref. 32). Although Paulson et al. (26) have discussed all three models in relation to T4 capsid length determination, they suggest that their data are most consistent with a Vernier mechanism. This mechanism envisages an elongation of both the capsid and core tubular parts until a preferred length is reached, defined as a state where the core and capsid lattices come into register. Stronger bonds between core and capsid would be formed at this level, halting further axial growth and initiating the formation of an end-cap. Such a mechanism of length regulation should depend on the structure of the proteins P22 and P23 but not on their relative availability.

Recent experiments (unpublished results) have shown, however, that mixed infections with T4D·22$^-$ (amE209) and T4D·23$^-$ (amB17) produce up to 30% isometric phage for a ratio of infection of 15 to 5. In this case, both the core and the capsid should be made exclusively of wild-type gene products rather than of proteins with an altered structure. The production of a significant proportion of isometric phage capsids could be explained by a reduced availability of P22 relative to P23 if the P23 shell had an intrinsic tendency to close in the absence of "support" from the P22 core, a possibility also considered by Paulson et al. (26).

Our previous finding that a mixed infection of wild-type and T4D·24 (amN65)-produced giants (4) weighs against the Vernier model since 1) these giants are made from wild-type gene products and 2) P24 is not present in proportion to P23* in the tubular part of the capsid in finished phage (4) or in $\tau$ particles (L. Onorato, unpublished findings). In our opinion, it is not possible to modify the Vernier model to account for the results of these two experiments and still retain the essential characteristics of the Vernier mechanism. Experiments are now under way in our laboratory to endeavour to establish a more satisfactory model for the T-even phage head length determination mechanism.

## ACKNOWLEDGMENTS

We would like to thank R. van den Broek for technical assistance and Drs. L. Onorato and M. K. Showe for many valuable suggestions and discussions concerning the results of this project. We thank Drs. T. G. Frey and R. van Driel for their critical reading of the manuscript. Professor E. Kellenberger, in whose laboratory this work was done, provided continual encouragement and many ideas.

We also thank the EDV Department of F. Hoffmann-La Roche, A. G. for providing our computing facilities without which an important part of the work could not have been done.

The project was supported in part by the Swiss National Science Foundation.

## REFERENCES

1. Doermann, A. H., Eiserling, F. A., and Boehner, L.: J. Virol. 12:374 (1973).
2. Doermann, A. H., Eiserling, F. A., and Boehner, L.: In "Virus Research," C. F. Fox and W. S. Robinson (Eds.). New York: Academic Press, p. 243 (1973).
3. Cummings, D. J., Chapman, V. A., De Long, S. S., and Couse, N. L.: Virology 54:245 (1973).
4. Bijlenga, R. K. L., Aebi, U., and Kellenberger, E.: J. Mol. Biol. 103:469 (1976).
5. Bolin, R. W., and Cummings, D. J.: J. Virol. 13:1368 (1974).
6. Bolin, R. W., and Cummings, D. J.: J. Virol. 13:1378 (1974).
7. Aebi, U., Bijlenga, R., van den Broek, J., van den Broek, R., Eiserling, F., Kellenberger, C., Kellenberger, E., Mesyanzhinov, V., Müller, L., Showe, M., Smith, R., and Steven, A.: J. Supramol. Struct. 2:253 (1974).
8. Ishii, T., and Yanagida, M.: J. Mol. Biol. 97:655 (1975).
9. Forrest, G. L., and Cummings, D. J.: J. Virol. 8:398 (1970).
10. Bijlenga, R.K.L., Scraba, D. and Kellenberger, E.: Virology 56:250 (1973).
11. Steven, A. C., Aebi, U., and Showe, M. K.: J. Mol. Biol. 102:373 (1976).
12. Steven, A. C., Couture, E., Aebi, U., and Showe, M. K.: J. Mol. Biol. 106:187 (1976).
13. Laemmli, U. K.: Nature 227:680 (1970).
14. Schreil, W. H.: J. Cell. Biol. 22:1 (1964).
15. Howard, Jr. G. W., Wolin, M. L., and Champe, S. P.: In Transactions of the New York Acad. Sci., Series II, 34:36 (1972).
16. Showe, M. K., Isobe, E., and Onorato, L.: J. Mol. Biol. 107:55 (1976).
17. Minagawa, T.: Virology 13:515 (1961).
18. Black, L. W., and Ahmad-Zadeh, C.: J. Mol. Biol. 57:71 (1971).
19. Coppo, A., Mangi, A., Pulitzer, J. F., and Takashashi, M.: J. Mol. Biol. 76:61 (1973).
20. Horwitz, H. R.: J. Mol. Biol. 90:727 (1974).
21. Horwitz, H. R.: J. Mol. Biol. 90:739 (1974).
22. Moody, M. F.: Virology 26:567 (1965).
23. Branton, D, and Klug, A.: J. Mol. Biol. 92:559 (1975).
24. Eiserling, F. A., Geiduschek, E. P., Epstein, R. H., and Metter, E. J.: J. Virol. 6:865 (1970).
25. Chao, J., Chao, L., and Speyes, J. F.: J. Mol. Biol. 85:41 (1974).
26. Paulson, J. R., Lazaroff, S., and Laemmli, U.K.: J. Mol. Biol. 103:155 (1976).
27. Aebi, U., van Driel, R., Bijlenga, R. K. L., ten Heggeler, B., van den Broek, R., Steven, A. C., and Smith, P. R.: J. Mol. Biol., in press.
28. Epstein, R. H., Bolle, A., Steinberg, C. M., Kellenberger, E., Boy de la Tour, E., Chevalley, R., Edgar, R. S., Susman, M., Denhardt, G. H., and Leilausis, A.: Cold Spring Harbor Symp. Quant. Biol. 28:375 (1963).
29. Laemmli, U. K., and Eiserling, F. A.: Molec. Gen. Genet. 101:333 (1968).
30. Laemmli, U. K., Molbert, E., Showe, M. K., and Kellenberger, E.: J. Mol. Biol. 49:99 (1970).
31. Black, L. W., and Brown, D. T.: J. Virol. 17:894 (1976).
32. Kellenberger, E.: In "Polymerization in Biological Systems." Ciba Foundation Symposium 7:295 (1972) ASP, Amsterdam.
33. Lake, J. A., and Leonard, K. R.: J. Mol. Biol. 86:499 (1974).

## APPENDIX: THE COMPUTER FILTRATION OF HEXAGONAL LATTICES
(P. R. Smith and U. Aebi)

### The Method

We pointed out elsewhere (1) that if a computer filtration is to perform a total rather than a local average over repeating structure digitised at the Nyquist rate, the reciprocal lattice of the structure should coincide with points sampled by the discrete Fourier transform (DFT). This requirement can be satisfied if the digitised area contains an integral number of unit cells with each unit cell sampled with an integral number of sample points. The success of a filtration of a square or rectangular lattice therefore hinges on the accuracy with which the image can be scaled and aligned with respect to the sampling grid, since once this is done the filtration is performed by setting to zero all DFT sample points not on the appropriate reciprocal lattice.

Hexagonal lattices represent an interesting variation of this problem because the lattice vectors intersect at 60° rather than 90°. Strictly following the prescription outlined above and given in detail in Aebi et al. (2) would require digitising the image on a hexagonal net. This causes practical difficulties because our Optronics rotating drum densitometer collects data on a square raster and could not be programmed to collect data on a hexagonal raster. Furthermore, a subsequent transfer of data by interpolation from the square raster on which it was collected to a hexagonal net is too inefficient computationally for serious consideration.

The alternative to hexagonal sampling is to sample the image with respect to the rectangular "superlattice" which contains two unit cells of the hexagonal lattice (see Fig. A1). Alignment and scaling is then done by fitting an integral number of these "superunit cells" onto a rectangular sampling grid containing an integral number of superunit cells in each direction and with each superunit cell sampled with an even number of sample points in both directions. Filtration of the DFT then consists of two steps: a) the setting to zero of all DFT samples not falling on the reciprocal lattice of the "superlattice," and b) the zeroing of every alternate spatial frequency in both directions as shown in Fig. A2; i.e., the zeroing of those super-reciprocal lattice points that were not also reciprocal lattice points of the hexagonal lattice. Three- and sixfold symmetrisation is done by averaging those coefficients in the transform related by this symmetry.

After reverse Fourier transformation a filtered lattice is obtained that is nearly hexagonal, differing only by a small scaling factor in the direction of the superlattice vector (which has to be scaled to an even number of samples).

The reverse transform is only able to show a three- or sixfold rotational symmetrization exactly on a few special points because, in general, points on the rectangular lattice are not interrelated by this symmetry. The reconstructed unit cells therefore represent the result of sampling an exact three- or sixfold unit cell on a rectangular sampling grid. Figure 4 in the preceding paper shows that the small departures from exact three- and sixfold symmetry resulting from subsequent bilinear interpolation are not discernible in the photowritten images.

### The T2 and T4 Giants

Filtering of the tubular part of a giant phage by the method outlined above is difficult to do in practice because relatively few unit cells (50) can be placed in the rectangular

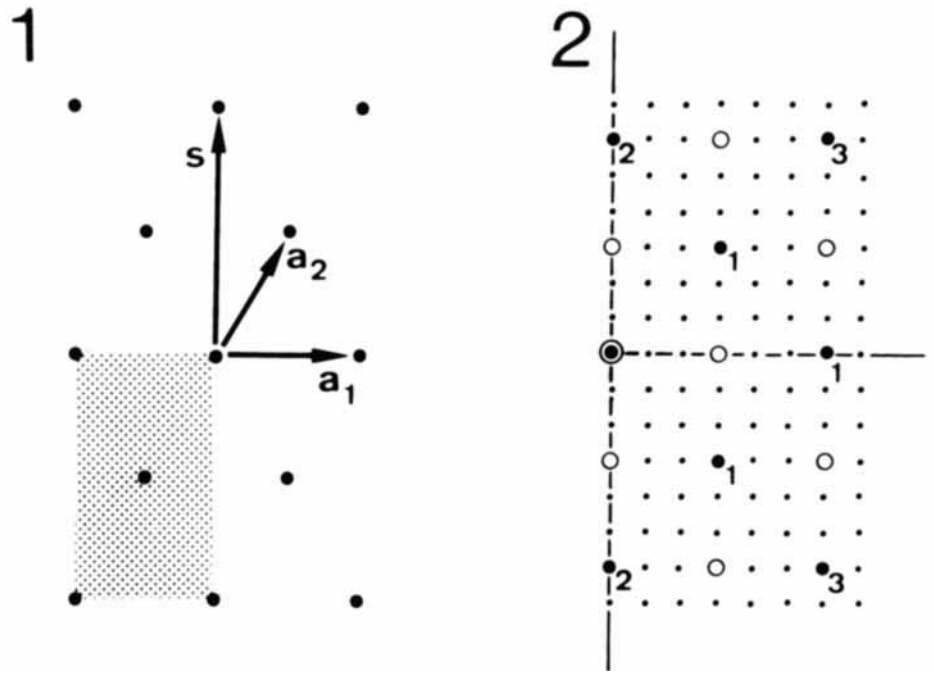


Fig. A1. An array of black dots arranged on a hexagonal lattice is shown together with their lattice vectors $a_1$ and $a_2$. The shaded area shows the so-called superunit cell which has lattice constants $a_1$ and $s$. In an ideal hexagonal lattice $|a_1| = |a_2|$ and $|s| = \sqrt{3}\cdot|a_1|$. In our case the T2 and T4 giants were scanned parallel to the $a_1$ vector and 32 samples were taken along its length: With this sampling $[s]$ is 55.42 sample points. The scaling along the s direction was altered by interpolation so that the superunit cell was sampled with 56 samples along its length. The use of an even number of samples in each direction ensures that the two hexagonal unit cells contained in the superunit cell are equivalently sampled.

Fig. A2. The array shows diagramatically the arrangement of the complex coefficients in computer storage resulting from a DFT of a correctly scaled digitised array of 3 X 3 superunit cells. The large black dots and the open circles together represent the reciprocal lattice of the superunit cell array. The small black dots represent Fourier coefficients rejected (zeroed) in a filtration, since they do not lie on points in the superunit cell reciprocal lattice. In order to average over the hexagonal lattice rather than the superlattice, the coefficients represented by open circles are also deleted: The only nonzero numbers remaining are indicated by the large black dots. The numbers beside each of these indicate the radial orders of the reciprocal hexagonal lattice (3) to which they belong. Three- or sixfold averaging is achieved by averaging over the symmetry-related coefficients; the three coefficients labeled 1, for example, together with their Friedel mates. The overall size of the array of DFT coefficients depends on the number of samples in the unit cell once the number of unit cells is fixed.

window sampled for filtration. This is unfortunate because 50 unit cells is nearly the smallest number of unit cells that, when averaged, give a reasonable signal-to-noise ratio in the filtration. The computed diffraction patterns are therefore very noisy and alignment and scaling is consequently difficult. Optimization of scaling and alignment was therefore done using the optical filtrations as a guide, since larger areas of giant heads could be optically filtered and consequently the signal-to-noise ratios for the optical filtrations were better.

In spite of the initially lower signal-to-noise ratio in the computer filtrations, they proved to be worthwhile for the following reasons. First, the computer filtration procedure was linear in all its steps, which is not necessarily the case in the optical filtration method. Second, the sixfold rotational symmetrization could be done in all cases. This was sometimes difficult to do by photographic superposition, because the small lattice ellipticities (deviations from an exact hexagonal lattice) limited the size of the regions that were effectively in register. Third, since in optical processing intensities are recorded, additional features due to contrast reversal may turn up in an optical filtration, depending on the mean background level chosen (how much of the zero-order intensity has been reduced in order to enhance the contrast in the filtered image) unless great care has been taken. This cannot happen in a computer filtration, since amplitudes rather than intensities are manipulated: the computer filtration therefore provides a check on the optical filtration. This was found to be useful in the case of filtrations of the T2L giants, where errors in stopping the zero order in the optical filtration often converted the deep minimum at the center of the capsomere into a central maximum.

## REFERENCES (Appendix)

1. Smith, P. R., and Aebi, U.: J. Supramol. Struct. 1:516 (1973).
2. Aebi, U., Smith, P. R., Dubochet, J., Henry, C., and Kellenberger, E.: J. Supramol. Struct. 1:498 (1973).
3. Steven, A. C., Aebi, U., and Showe, M. K.: J. Mol. Biol. 102:373 (1976).